Materials Today Bio 17 (2022) 100487

Contents lists available at ScienceDirect

Materials Today Bio

journal homepage: www.journals.elsevier.com/materials-today-bio

DLP-based bioprinting of void-forming hydrogels for enhanced stem-cell-mediated bone regeneration

Jie Tao [a,1], Shunyao Zhu [a,1], Xueyuan Liao [a], Yu Wang [a], Nazi Zhou [a], Zhan Li [b], Haoyuan Wan [a], Yaping Tang [a], Sen Yang [a], Ting Du [d], Yang Yang [a], Jinlin Song [c,**], Rui Liu [a,*]

[a] Department of Stomatology, Daping Hospital, Army Medical University (The Third Military Medical University), Chongqing, 400042, China
[b] Department of Stem Cell and Regenerative Medicine, State Key Laboratory of Trauma, Burn and Combined Injury, Daping Hospital, Army Medical University, Chongqing, 400042, China
[c] College of Stomatology, Chongqing Medical University, Chongqing, China
[d] Non-coding RNA and Drug Discovery Key Laboratory of Sichuan Province, Chengdu Medical College, Chengdu, Sichuan, China

ARTICLE INFO

Keywords:
3D bioprinting
Void-forming
Macroporous hydrogel
Bone marrow stem cells
Bone regeneration

ABSTRACT

The integration of 3D bioprinting and stem cells is of great promise in facilitating the reconstruction of cranial defects. However, the effectiveness of the scaffolds has been hampered by the limited cell behavior and functions. Herein, a therapeutic cell-laden hydrogel for bone regeneration is therefore developed through the design of a void-forming hydrogel. This hydrogel is prepared by digital light processing (DLP)-based bioprinting of the bone marrow stem cells (BMSCs) mixed with gelatin methacrylate (GelMA)/dextran emulsion. The 3D-bioprinted hydrogel can not only promote the proliferation, migration, and spreading of the encapsulated BMSCs, but also stimulate the YAP signal pathway, thus leading to the enhanced osteogenic differentiation of BMSCs. In addition, the in vivo therapeutic assessments reveal that the void-forming hydrogel shows great potential for BMSCs delivery and can significantly promote bone regeneration. These findings suggest that the unique 3D-bioprinted void-forming hydrogels are promising candidates for applications in bone regeneration.

1. Introduction

Bone defects, causing more than 1.5 million new grafts in the USA annually, remain the most pressing challenge in regenerative medicine [1]. Despite the capacity of the bone to rejuvenate itself, the regeneration potential is interrupted in the case of critical-sized defects and a tissue-engineered graft is generally required for bone tissue remolding. By far, the traditional treatment still cannot satisfy the increasing clinical demand for effective bone grafts due to the limited availability (in the case of autograft), risk of pathogen transmission (in the case of allograft), and reduced healing potential (in the case of biomaterial-based scaffolds) [2], which impel us to search for better alternatives. In the bone healing process, complex biological issues occur including inflammation response, new blood vessel formation, recruitment of osteogenic cells etc [3,4]. Research has demonstrated that a well-designed microenvironment that can regulate these issues is essential in bone regeneration [5,6]. In light of this, there is a great need to develop functional and bioactive tissue-engineered scaffolds that might bring new prospects to regulate the interaction between the implants and host tissues for the regeneration of bone defects.

Bone marrow stem cells (BMSCs) that localize in the stromal compartment of the bone marrow are characterized by the abilities of self-renewal and differentiating into specialized cells, opening a promising avenue in regenerative medicine [7]. Over the past decades, a number of tissue engineering approaches combined with BMSCs have been used in clinical practice for the treatment of bone defects [8]. The installed stem cells can assist bone tissue regeneration through differentiation into osteoblasts, recruitment of other therapeutic cells, or building a favorable microenvironment *via* the release of paracrine factors [9,10]. However, direct delivery of cell suspension to the sites of bone fracture generally brings a disappointed outcome because of the low survival rate, short retention, and restricted functions. Recently, there increased an attention to the creation of hydrogel constructs containing stem cells for the treatment of bone defects, including silk fibroin,

* Corresponding author.
** Corresponding author.
E-mail addresses: songjinlin@hospital.cqmu.edu.cn (J. Song), dentistliurui@163.com (R. Liu).
[1] These authors contributed equally to this work.

https://doi.org/10.1016/j.mtbio.2022.100487
Received 8 September 2022; Received in revised form 31 October 2022; Accepted 3 November 2022
Available online 5 November 2022

alginate, and GelMA [11]. GelMA, which is functionalized with photosensitive groups on gelatin backbone, not only shows favorable abilities in facilitating the adhesion and proliferation of BMSCs [12], but also owns tunable mechanical properties by photopolymerization. Meanwhile, the microenvironment constructed by GelMA hydrogel favors the osteogenesis of encapsulated BMSCs [13,14], showing potential for bone regeneration. However, GelMA hydrogels that retain structurally stable generally have a high crosslinked degree and dense polymer network, leading to insufficient nutrient diffusion and restricted cell migration/-proliferation [15]. As reported by the previous studies [16,17], hydrogels with relaxation properties could promote the viability and functions of the encapsulated stem cells, leading to enhanced efficiency. However, the stress relaxation relied on the breakage of the hydrogel network, leading to disappointing structural integrity and mechanical properties, which is not an ideal biophysical element in bone regeneration.

3D bioprinting technologies have attracted much attention in fabricating high-performance bone tissue constructs [18,19]. They enable a high level of spatiotemporal modulation of the interactions between cell-cell and cell-extracellular matrix (ECM) to produce structurally sophisticated and functionally relevant tissue constructs. To date, extrusion-based bioprinting technology has been the most widely used for preparing bone tissue constructs owing to its advantages of widespread availability, cost-effectiveness, simplicity, and facile processing [20]. However, due to the interfacial artifacts between the printing lines and the serial writing fashion, the structural integrity and fabrication speed of the bone tissue constructs are compromised by the extrusion-based bioprinting technology, restricting their clinical applications. By comparison, constructs fabricated by digital light processing (DLP)-based 3D bioprinting platform are characterized by superior speed, resolution, and structural integration [21]. Zhang et al. developed a haversian bone-mimicking construct to foster the formation of new bone and blood vessels by DLP-based printing technology [22], demonstrating the potential of using this advanced 3D printing technology to build bone tissue constructs.

Here, we investigate the potential of a void-forming hydrogel to regulate the behavior and functions of the encapsulated BMSCs for bone tissue regeneration *via* a DLP-based 3D bioprinting platform (Fig. 1). We hypothesize that bioprinted void-forming hydrogels can not only offer porous structure for cell spreading, but also enable a cell-inspired microenvironment for preserving and enhancing the functions of encapsulated stem cells. The efficacy of the construct was examined to repair a 6 mm cranial defect. This construct could promote the formation of new bone tissues, contributing to clinical applications.

2. Materials and method

2.1. Materials

Gelatin and methacrylic anhydride were purchased from Sigma Aldrich. Dextran (average Mw = 500, 000) was purchased from J&K Scientific. Cell Counting Kit-8 (CCK-8) was purchased from MCE. Live/Dead assay kit was purchased from KeyGEN BioTECH. Alexa Fluor™ 488 Phalloidin and 4',6-diamidino-2-phenylindole (DAPI) were purchased from Thermo Fisher. Gelatin methacryloyl (GelMA) and lithium phenyl-2,4,6-trimethyl-benzoylphosphinate (LAP) were synthesized according to previous study [23]. Primary antibodies (anti-OCN and anti-COL-1) were bought from Affinity Biosciences and anti-YAP were bought from Cell Signaling Technology.

2.2. Cell culture

Bone mesenchymal stem cells (BMSCs) used for fabricating cellular hydrogels were isolated from adult rat. The method for the isolation of BMSCs was according to the previous study. The isolated BMSCs were cultured in DMEM/F12 (Gibco) supplemented with 10% (v/v) fetal bovine serum (FBS, Gibco) and 1% (v/v) penicillin/streptomycin (BI). All the cells were cultured into a humidified incubator with 5% CO_2 atmosphere at 37 °C.

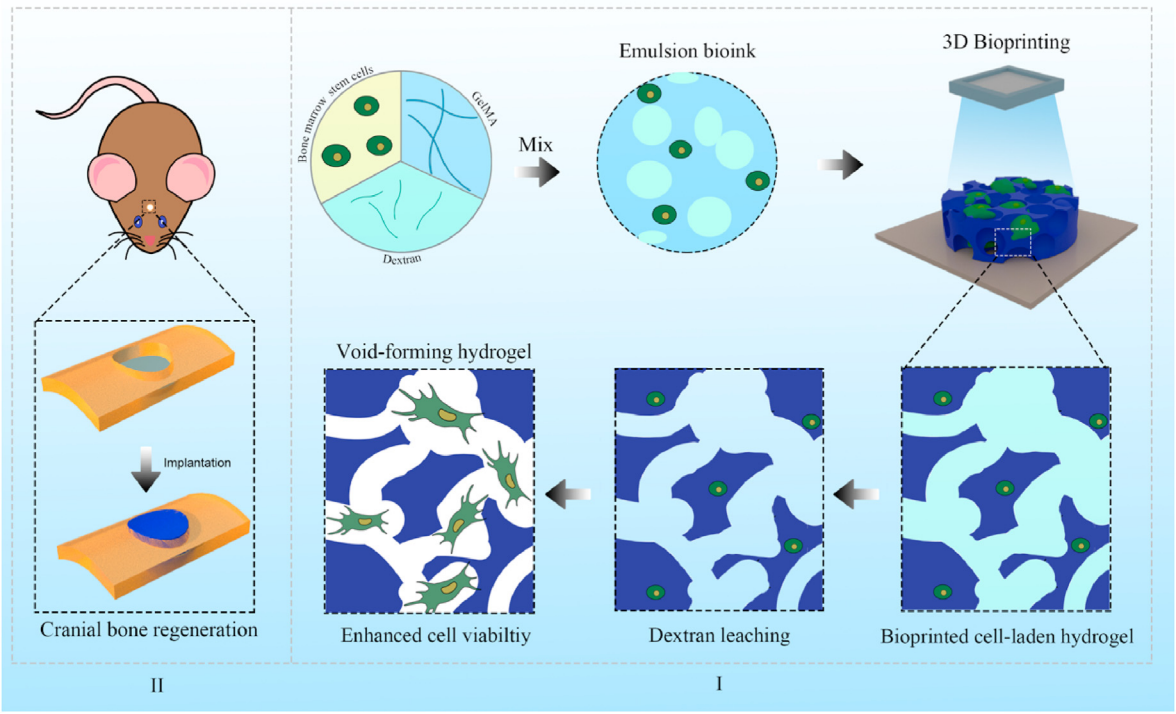

Fig. 1. Schematic illustration of the 3D-bioprinted void-forming hydrogel constructs for implantation. I) An aqueous emulsion bioink, in which dextran solution drop-like distributes within GelMA solution, was prepared by the mixture of GelMA, Dextran, and stem cells for 3D bioprinting of void forming hydrogel to II) repair the cranial defect.

2.3. Void-forming hydrogel fabrication and characterization

The void-forming hydrogels were prepared by DLP-based 3D printing of aqueous emulsion composed of the mixture of dextran solution and GelMA solution with a volume ratio of 1:2 according to our previous study [24]. Briefly, the dextran and GelMA polymers were dissolved into PBS solution to form 10% (w/v) dextran solution (average Mw = 500, 000; without modification) and 15% (w/v) GelMA solution at room temperature, separately. Then, 0.5% (w/v) of photo-initiator (LAP) was respectively added the solution before construction by DLP-based 3D printing using 405 nm visible light (60 mW/cm^2). Pure GelMA hydrogel was settled as the control group.

To observe the pore size and distribution within 3D-printed hydrogels in their hydrated state, rhodamine-labeled GelMA was used. 15% (w/v) of rhodamine labeled GelMA solution was gently mixed with 10% (w/v) of dextran solution. And the hydrogel preparation procedure was the same as previous. The hydrated morphology of the hydrogels was assessed by laser confocal microscopy (Leica SP8).

The micromorphology of the 3D-printed hydrogels was observed by a scanning electron microscopy (SEM, SU8020, Hitachi). The printed hydrogels were treated with gradual dehydration in ethanol (30%, 45%, 60%, 75%, 90%, 100%), critical point drying, and Pt/C-shadowing before we visualized the hydrogels. Compression properties was measured using mechanical testing machine at room temperature (ElectroForce, TA).

The permeability of the printed hydrogels was evaluated as following. A cylinder-shaped hydrogel containing FITC-labeled BSA was prepared using DLP-based 3D printer and incubated into culture medium. At predesigned timepoint, the hydrogels were imaged by florescent microscopy.

To evaluate the degradation properties of the printed hydrogel, the obtained samples were washed with PBS for 24 h (37 °C) to remove the photoinitiator and uncrosslinked polymers. The degradation of the printed hydrogels was imaged followed immersed in collagenase solution. The degradation of the hydrogel was calculated as a ratio of the loss area to the primary area.

2.4. 3D printing of cellular void-forming hydrogels

The collected BMSCs were resuspended into GelMA solution (15%, w/v) and mixed with dextran solution (10%, w/v) at a volume ratio of 2:1. The prepared bioink was constructed into designer hydrogels *via* DLP-based 3D printing technology (Movie S1). The bioprinter was settled in the clean bench and was sterilized using UV light for 30 min before bioprinting. The printing parameters were used as follows: printing speed, 0.1 mm/s; UV light intensity, 60 mW/cm^2. The entire hydrogels measured around 6 mm in diameter and 1 mm in thickness. After washed with PBS for three times, the 3D-printed cellular hydrogels were cultured into a humidified incubator with 5% CO_2 atmosphere at 37 °C.

Supplementary data related to this article can be found at https://doi.org/10.1016/j.mtbio.2022.100487.

The viability of the encapsulated BMSCs was measured by live/dead assay and CCK-8 assay according to the manufacturer's instructions. To observe the spreading of the encapsulated BMSCs within the void-forming hydrogels, the cultured hydrogels were washed with PBS for several times and fixed by 4% paraformaldehyde. The cytoskeleton and nucleus were stained with Alexa 488-phalloidin and DAPI, separately. The cell spreading was visualized using laser confocal microscopy.

Immunofluorescent staining was performed on encapsulated BMSCs with the 3D-bioprinted hydrogels after 7 days of culture. The primary antibody against YAP (1:100) was utilized.

To assess the effect of porous structure on osteogenic differentiation, the printed hydrogels were osteoin-duced in osteogenic medium (Cyagen, China). After 7 d and 14 d of osteoinduction, quantitative real-time PCR (qRT-PCR) was employed to evaluate the mRNA expression of the encapsulated BMSCs. Total cellular RNA was extracted of the cells using Trizol and reverse-transcribed into cDNA using All-In-One 5X RT MasterMix (Applied Biological Materials). Assays were performed using BlasTaqTM 2X qPCR Master Mix (Bio-Rad, Thermo scientific). The primers are listed in Table 1.

2.5. Migration and differentiation of the encapsulated cells

The migration performance of encapsulated BMSCs was tested by Transwell assays. Transwell assays were evaluated in 12-well plate Transwell with a diameter of 12 mm and a pore size of 8 μm. The cellular hydrogels were placed in the upper chambers. After 5 and 10 days, the migrated cells were fixed with 4% paraformaldehyde for 10 min, and the cells remaining on the top of the Transwell membranes were removed. The migrated cells were stained with crystal violet and imaged with inverted microscope.

The alkaline phosphatase (ALP) activity of the encapsulated BMSCs within the 3D-printed hydrogels was measured after incubation for 7 and 14 days. The osteogenic differentiation medium with osteoinductive factors was refreshed every two days. At prescribed time, the 3D-printed cellular hydrogels were washed with PBS and lysed with collagenase and RIPA lysis buffer. The ALP activity was measured using Alkaline Phosphatase Assay Kit at the wavelength of 405 nm. The total protein level was determined by BCA Protein Assay Kit. The study was performed in triplicate. Meanwhile, the qRT-PCR was employed to analysis the osteogenic expression. The primers are listed in Table 1.

2.6. Surgical process

All animals were purchased from the laboratory Animal Center of Army Medical University. Rat were acclimatized to the environment of the animal facility for at least seven days prior to the experiments. The animal protocol used in this study was carried out in accordance with the guidelines for the care and use of laboratory animals published by the ministry of health of the People's Republic of China and was approved by the Institutional Animal Care and Use Committee of the Army Medical University (AMUWEC20211834). To evaluate the efficacy of cellular hydrogels, full-thickness craniotomy defects (6 mm diameter) were created in the parietal bone of rats (200–220 g, male). The rats were randomly divided into three groups: Void-forming group (n = 6), Standard group (n = 6) and Control group (n = 6). Each of group of rats was anesthetized with intraperitoneal injection of chloral hydrate solution (0.3 mL/100 g). For rats in the control group, the created defects had no treatment. The cranial defect treated with 3D-printed BMSCs-laden void-forming hydrogels or 3D-printed BMSCs-laden standard hydrogels was regarded as void-forming group or standard group. After 8 weeks, the rats were sacrificed, and the harvested samples were fixed with 4% paraformaldehyde for over 24 h.

2.7. Micro-computed tomography (micro-CT)

The fixed samples were scanned with micro-CT (PerkinElmer). Three-dimensional reconstruction was performed using the Sky Scan CtAn softeware and the newly formed bone area was measured by Image J software.

Table 1
Real-time PCR primers used in this experiment.

Gene name	Primer Forward	Primer Reverse
RUNX2	CTTCGTCAGCGTCCTATCAGTTC	CAGCGTCAACACCATCATTCTG
OSX	CCACCAAGAATTACTCAGAACCC	AAGGACCGACTCACTCAGTCT
CYR61	AGAGGCTTCCTGTCTTTGGC	CTCGTGTGGAGATGCCAGTT
CTGF	CCCAACTATGATGCGAGCCA	GACGACTCTGCTTCTCCAGC
CDH2	GCGGGGAAGAGGCCAAATTA	GTCAGAGTGTCGAGGAGACG
GAPDH	TGTGAACGGATTTGGCCGTA	ACTGTGCCGTTGAATTTGCC

2.8. Histological evaluation

After micro-CT scanning, the samples were decalcified for further histological evaluations. The decalcified samples were dehydrated through an ascending graded series of ethanol solutions and cleared with xylene. Then the samples were embedded in paraffin and sectioned at a thickness of 5 μm for histological evaluations. Hematoxylin & eosin (H&E), Masson trichrome and immunohistochemistry (COL-1, 1:100 and OCN, 1:100) staining were carried out *via* standard protocols and imaged using an optical microscope.

2.9. Statistical analysis

All statistical analysis was conducted using Graphpad Prim 9 (Graphpad Software Inc.). The significance was measured using one-way ANOVA or two-way ANOVA. Results were displayed as means with standard deviation (SD) and $p < 0.05$ was considered as statistically significant. For all the tests, data from at least three independent samples or experiment repeated thrice were used.

3. Results

To address the limitations of current BMSCs-based biomaterials in the treatment of critical bone defects, the present study, therefore, developed a void-forming hydrogel by 3D-bioprinting of a mixture of an emulsion solution and BMSCs. The aqueous emulsion was consisted of two immiscible phases (GelMA and dextran), in which dextran microdroplets dispersed within GelMA solution (Fig. S1, Supporting Information). The emulsion was polymerized and constructed using a DLP-based bioprinter (Fig. 2A). A visible light (405 nm) was used to induce the polymerization of the emulsion. The printing process was realized by continuously projecting the digital images and lifting the polymerized hydrogels. After fabrication, the dextran phase could be removed *via* dissolving into water or incubation medium, leaving pores within the GelMA hydrogels. The 3D-printed hydrogels were visualized with laser confocal microscope. The pure GelMA solution used for preparing the standard hydrogel was treated as the control group. Rhodamine B-labeled GelMA and FITC-labeled dextran polymers were used to image the hydrate morphology of the hydrogels. As shown in Fig. 2B–i, the hydrogel emitted red fluorescence represented GelMA polymer networks, while dark areas indicated the formed pores, implying the successful preparation of 3D-printed porous hydrogels. The void-forming hydrogels and standard hydrogels were further critical-point drying and characterized with scanning electron microscope (SEM, Fig. 2B–ii). The standard hydrogels had a smooth surface, and no pores were found on the hydrogels. As we hypothesized, porous structure displayed across all the void-forming hydrogels in consistent with fluorescent images. The above results indicated that the dextran phases could be removed to leave pores within the GelMA hydrogels. The effect of the formed pores on the mechanical properties was using a mechanical analyzer in the unconfined compression mode. The porous structure led to the decreased strain and stress of the hydrogels, compared to the standard hydrogels (Fig. 2C; Fig. S2). Meanwhile, the void-forming hydrogel degraded faster than standard GelMA hydrogel in the presence of collagenase (Fig. S3). Next, the release test of the void-forming hydrogels was evaluated by mixing the FITC-labeled BSA with the emulsion or pure GelMA solution. As presented in Fig. 2D, comparing to the standard hydrogels, the FITC-labeled BSA could diffuse faster from the void-forming hydrogels, indicating that these hydrogels promoted the exchange of substance between the encapsulated cells and extracellular microenvironment.

As high cell viability is a premise for successful bioprinting of constructs in bone regeneration, live/dead assay and CCK-8 are performed to investigate the effects of pore formation on encapsulated cell viability and distribution within the void-forming hydrogels. A live/dead fluorescent staining post-printing revealed that both 3D-printed hydrogels had no toxicity on the encapsulated cells within 5 days (Fig. 3A).

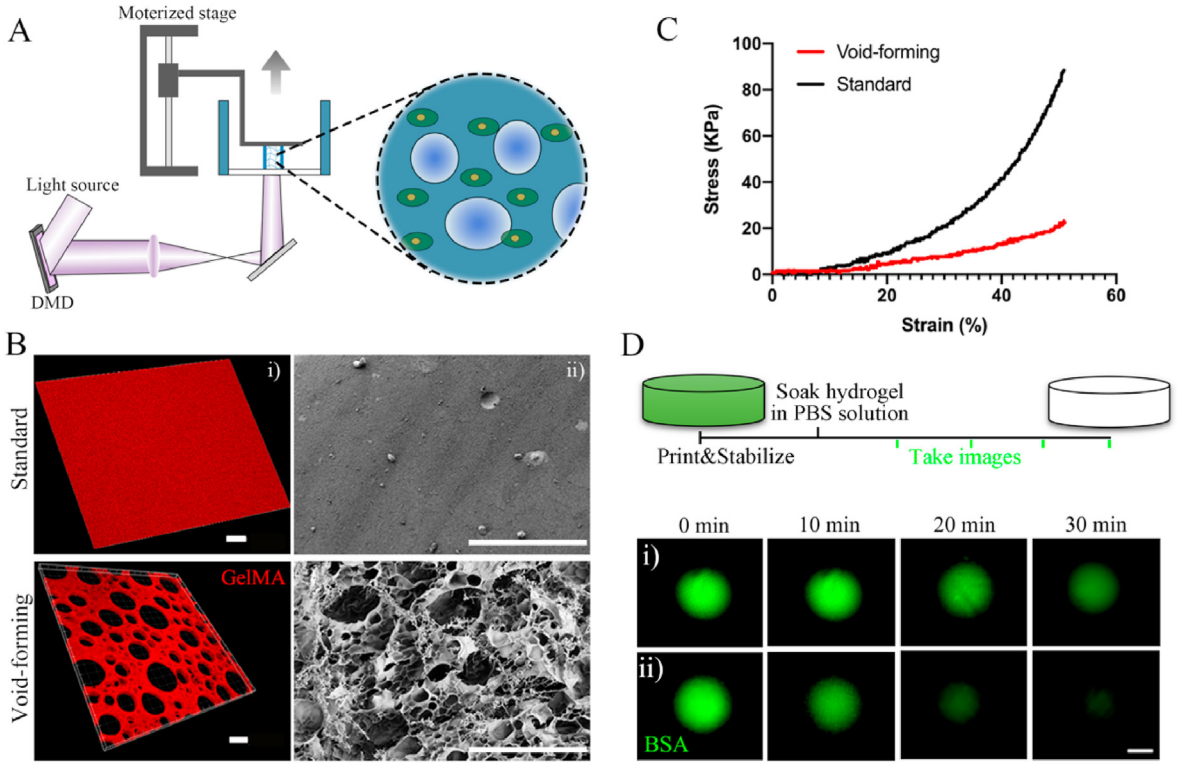

Fig. 2. 3D bioprinting of void-forming hydrogels. (A) Schematic diagram of the DLP-based bioprinting approach. (B) Fluorescence microscopy (i, scale bar: 30 μm) and SEM (ii, scale bar: 100 μm) images of 3D-printed hydrogels. (C) Compressive stress-strain curve of 3D-printed hydrogels. (D) Diffusion of the BSA from the hydrogels (scale bar: 200 μm).

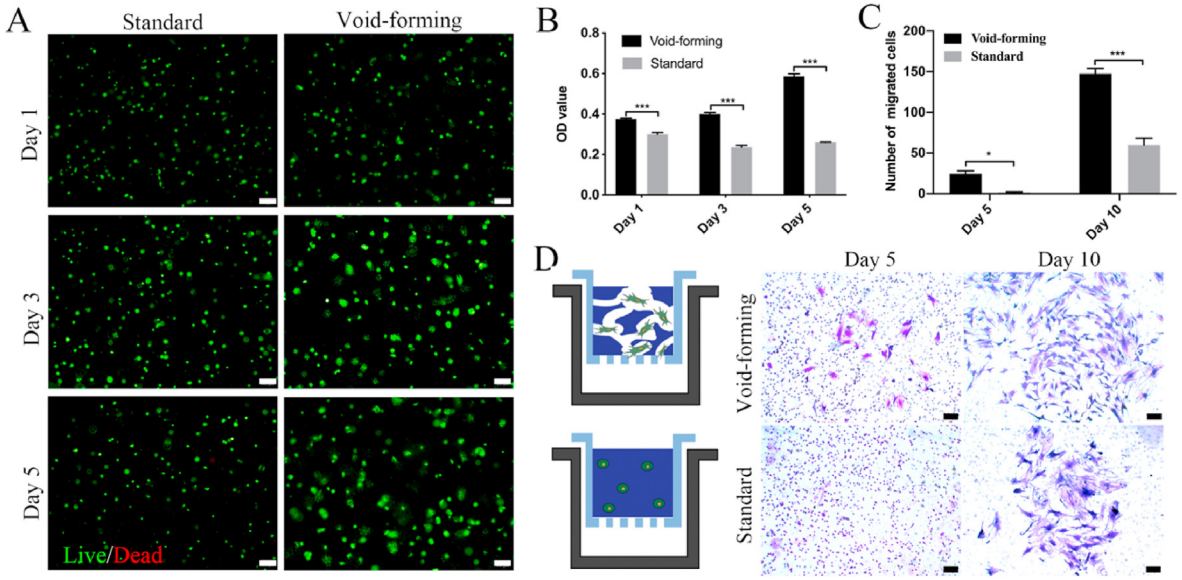

Fig. 3. The bioactivity of the encapsulated cells in 3D-bioprinted hydrogels. (A) Fluorescent images of live/dead stained BMSCs within printed hydrogels (scale bar: 100 μm). (B) Cell viability after incubation for 1, 3, and 5 days using CCK-8 assay (mean ± SD, n = 3, two-way ANOVA). (C) The quantitative analysis of migrated cells (mean ± SD, n = 3, two-way ANOVA). (D) Images of migrated BMSCs after 5 and 10 days of culture (scale bar: 100 μm). *P < 0.05, ***P < 0.001.

Meanwhile, it revealed that aggregated cells were rarely observed in both groups, demonstrating the good biodistribution of the encapsulated BMSCs in the printed hydrogels. Higher OD value indicates more cells. As shown in Fig. 3B, the proliferation of BMSCs was promoted within the void-forming hydrogels, while the standard hydrogels restricted the proliferation of encapsulated BMSCs and there was a slight decrease in

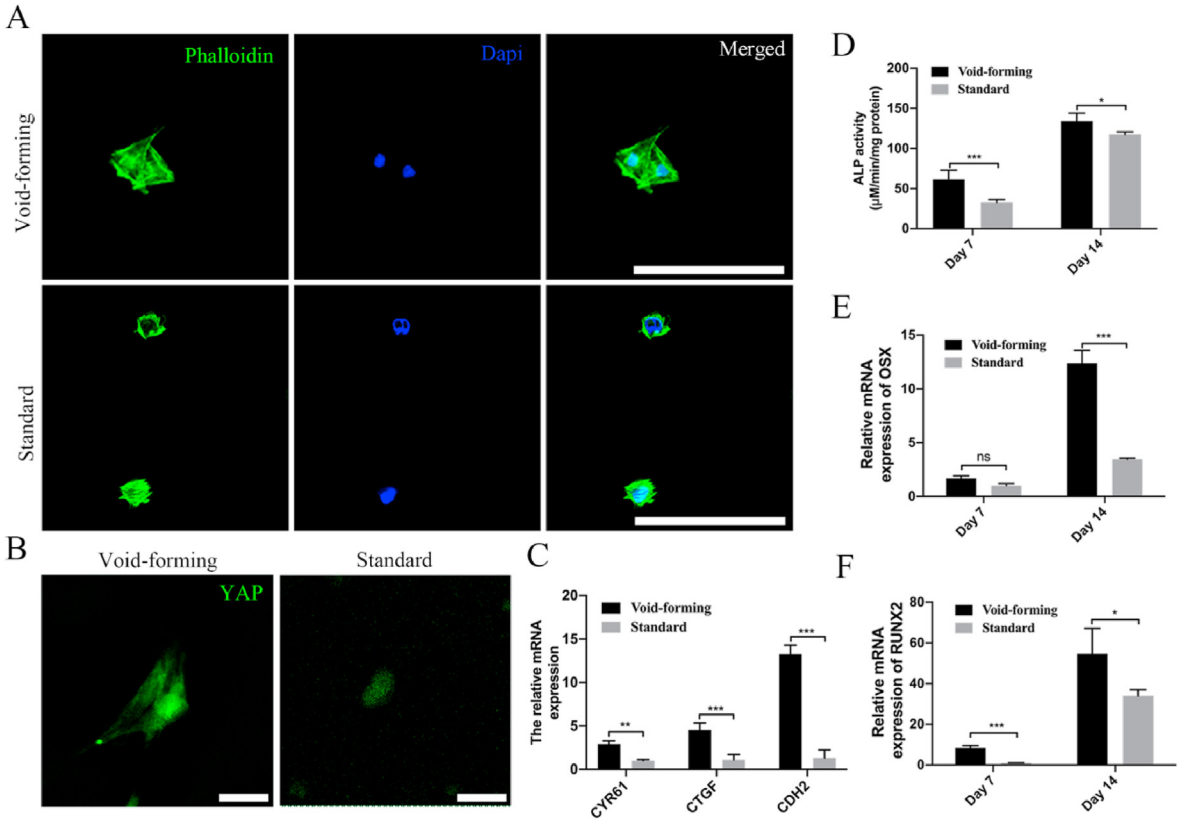

Fig. 4. 3D bioprinting of void-forming hydrogels promote cell-scaffold interaction. (A) Cell spreading within the printed hydrogels at day 7 (scale bar: 100 μm). (B) Representative immunofluorescence for YAP distribution in BMSCs (scale bar: 25 μm). (C) Quantification of gene expression of YAP targeted genes (CYR61, CTGF, and CDH2) after 7 days of culture (mean ± SD, n = 3, two-way ANOVA). (D) ALP activity of the encapsulated BMSCs at day 7 and 14 (mean ± SD, n = 3, two-way ANOVA). Summarized data showing the effect of porous structure on mRNA expression of (E) osteogenic differentiation related genes including osterix (OSX) and (F) runt-related transcription factor 2 (RUNX2) at day 7 and 14 (mean ± SD, n = 3, two-way ANOVA). Ns was determined as P > 0.05 with no statistical difference, *P < 0.05, **P < 0.01, ***P < 0.001.

cell number. To further demonstrate the advantages of the void-forming hydrogels on encapsulated stem cells, a migration assay was employed by gelling the cell-laden emulsion in the upper chamber of a transwell. As shown in Fig. 3C (Fig. 3D), the generated pores within the printed hydrogels caused more cells to migrate through the insert membrane, comparing to the standard hydrogels. These observations suggested that the void-forming hydrogels had the potential as the matrix for encapsulating BMSCs in bone tissue engineering.

Furthermore, there was considerable variation in spreading morphology for encapsulated BMSCs (Fig. 4A). Specifically, the area of spreading BMSCs was higher in void-forming hydrogels than that in standard hydrogels (Fig. S4, Supporting Information). BMSCs within the void-forming hydrogels exhibited extended spreading morphology. In contrast, the BMSCs remained rounded in the standard hydrogels. To investigate how cells respond to the void-forming hydrogel, nuclear localization of YAP transcriptional regulator was studied. The YAP transcriptional regulator was thought to play a vital role in controlling the cell fate in response to mechanical or geometric cues [25,26]. Nuclear localization of YAP was previously found to promote the cytoskeletal organization, paracrine regulation, and osteogenic differentiation of MSCs cultured on PLCL-nHA composite porous scaffolds [27]. The results presented in Fig. 4B displayed that the void-forming hydrogels could significantly promote YAP expression than that in standard hydrogels. In addition, there was more YAP expressed in nuclear in void-forming hydrogels, leading to the up-regulation of the YAP targeted genes CTGF, CYR61, and CDH2 (Fig. 4C), while YAP mainly remained in the cytoplasm in standard hydrogels. These results indicated that hydrogels in situ forming pores had an impact on transcriptional factor activity.

Based on the finding of promoted migration, proliferation, and cell spreading of encapsulated BMSCs within void-forming hydrogels, we next investigated the effect of pores on the osteogenic differentiation of encapsulated BMSCs. Alkaline phosphatase (ALP) plays a vital role

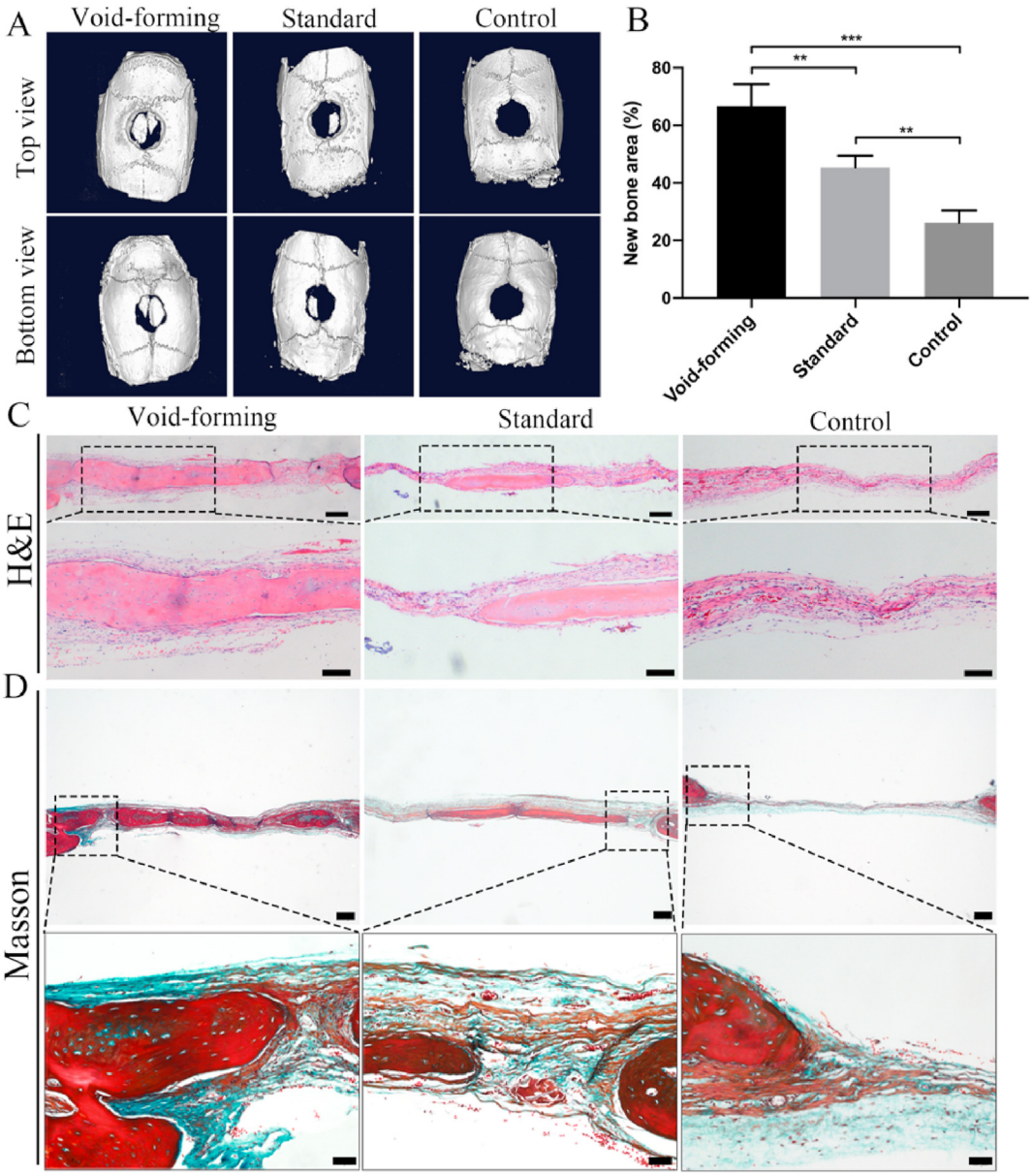

Fig. 5. In vivo evaluation of bone regeneration after void-forming hydrogels treatment using cranial defects in a rat model. (A) 3D reconstruction micro-CT images showing regenerated bone around the defects without treatment and those treated with standard and void-forming 3D-bioprinted hydrogels constructs. (B) Quantification of the area of newly formed bone (mean ± SD, n = 6, one-way ANOVA). Representative (C) H&E (scale bar at low magnification: 200 μm, scale bar at high magnification: 100 μm) and (D) Masson staining images of the regenerated bone tissues (scale bar at low magnification: 200 μm, scale bar at high magnification: 50 μm). **P < 0.01, ***P < 0.001.

during the early stage of osteogenesis. As shown in Fig. 4D, the expression of ALP was increased within 14 days in all groups and void-forming further enhanced ALP activity, which was significantly higher than that measured in standard hydrogels. We also analyzed the gene expression of osteogenic markers (OSX and RUNX2). For OSX, there presented a significant increase within the space of two weeks (Fig. 4E). At day 7, we found the OSX expression had no significant difference between the two groups. At day 14, the average OSX expression level was approximately 4-fold higher for void-forming hydrogels compared with the standard hydrogels. RUNX2 is the earliest and most specific marker for bone formation. Compared with standard hydrogels, the encapsulated BMSCs within void-forming hydrogels exhibited approximately 3-fold higher and 1.5-fold higher expression of RUNX2 at day 7 and 14, respectively (Fig. 4F). Our results demonstrated that directly 3D-printing of BMSCs-laden void-forming hydrogels had the potential in boosting bone regeneration.

To evaluate the efficacy of our void-forming hydrogels, we used these hydrogels to repair a rat cranial defect in vivo. Sprague–Dawley rats with cranial defects were randomly divided into three groups: void-forming, standard and control group. After 8 weeks post-implantation, the samples were harvested and fixed by 4% paraformaldehyde for radiological and histological evaluation. Fig. 5A displayed the micro-CT scanning images of the regenerated bone tissues. We found that newly generated bone tissues in the original cylindrical defects were observed. The generated bone tissues almost filled the defects in the void-forming group, while only a small amount of new bone tissues was observed in other two groups. In the quantitative micro-CT analysis (Fig. 5B), the defects treated with void-forming hydrogels and standard hydrogels were covered by newly formed bone at 67% and 45%, respectively, while the defects left empty showed a minimal healing (26%, control group). Moreover, the value of newly formed bone area in void-forming group was significantly higher than that in the standard group, demonstrating that void-forming hydrogels were more efficient at facilitating new bone tissue regeneration.

Moreover, the newly formed bone tissues were performed with histological staining (Hematoxylin &eosin and Masson's trichrome) to support the radiographic findings. As observed by H&E staining (Fig. 5C), the defect treated with void-forming hydrogel was occupied with newly formed bone, and thick tissue and bone-like tissue bridged the gaps. Meanwhile, void-forming group presented more newly formed bone tissues in the defects than standard group. In contrast, the defects in the control group were connected with fibrous inflammatory tissue. Masson trichrome staining images (red indicates calcified bone) displayed that the defect in the void-forming group was composed with blue and red stained osteoid islands (Fig. 5D), suggesting that the newly formed bone tissue gradually calcified and matured. In the standard group, the defect only filled with fibrous soft tissue with minimal bone formation. In addition, the formed pores within 3D-printed hydrogels that affected the newly formed bone tissues were also identified with immunohistochemical staining for osteogenic markers: collagen 1 (COL-1) and osteocalcin (OCN). According to the immunohistochemical results (Fig. 6), more osteogenic markers (COL-1 and OCN) were found in the void-forming group than other groups. Taken together, these results indicated that the directly 3D printing of porous hydrogels could facilitate BMSCs in repairing cranial defects.

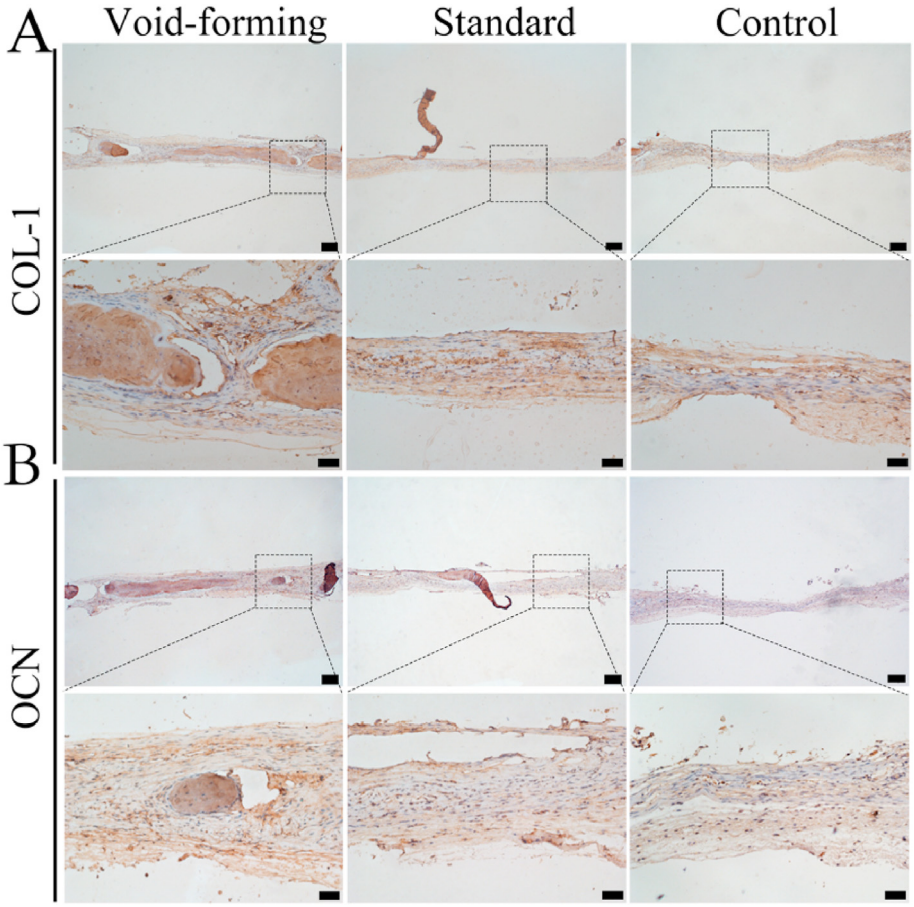

Fig. 6. Representative images for immunohistochemical staining of COL-1 (A) and OCN (B). (scale bar at low magnification: 200 μm, scale bar at high magnification: 50 μm).

4. Discussion

Bone tissue engineering has merged as a potent approach for the treatment of cranial defects to overcome the limitations of autografts and allografts, such as multiple surgeries, high risk of contamination, and lack of available donor sites [28]. This approach exploits a combination of cells, biomaterials, and growth factors to build biochemical and biophysical cues for rebuilding the lost bone tissues [29,30]. Meanwhile, inspired by the off-the-shelf availability, non-immunogenicity, and stability after *in vitro* expansion, BMSCs are currently the most promising cellular source to combine with other biomaterials for enhanced therapeutic index [31]. The implanted BMSCs can contribute to the fracture healing process *via* both cellular and paracrine effects, while biomaterials offer an optimized 3D space to preserve the functionalities of the contained BMSCs and provide physiological regulatory capacities for enhanced therapeutic efficacy. Nonetheless, traditional fabrication techniques generally can offer bone tissue constructs with simple architectures and hardly replicate microscale units of the natural bone tissues. And cells are commonly loaded after the establishment of constructs, leading to limited control over distribution. Recently, 3D printing of hydrogels for BMSCs delivery has received much attention in bone regeneration, in which 3D printing technology displays feasibility in patterning cells and biomaterials at high resolution for the creation of customized structure similar to bone tissues [32,33]. However, the therapeutic efficacy of the encapsulated stem cells can be dramatically inhibited by the inefficient substance exchange with external microenvironment and mechanical compression by the dense chemical-crosslinking polymers when directly 3D bioprinting of cell-laden hydrogels. Thus, a cell-inspired platform for enhancing the BMSCs behaviors and functions was appealing for bone regeneration.

3D printing of porous hydrogels containing BMSCs would be an ideal route of administration to the target sites for speeding up the bone regeneration. The contact between the structured porous hydrogels and surrounding tissues can significantly promote tissue ingrowth, angiogenesis, and interface fusion [24,34]. Although a number of porous hydrogels have been reported *via* salt-leaching [35], organic phases that served as porogens [36], and cryogelation [37], which are not ideal to be applied in 3D direct bioprinting of cell-laden porous hydrogels, as it was not possible to encapsulate living cells within polymer solution during the biofabrication process. In addition, cell seeding that was applied after the porous hydrogel establishment would lead to nonuniform distribution. Recently, the group of Zhang reported a cryobioprinting strategy to fabricate cell-laden porous hydrogel constructs [38], which used a freezing plate with controlled temperature. During the biofabrication process, the ice crystals were formed to serve as the porogens. And DMSO and melezitose must be added into the bioink to maintain the cell viability. To address these limitations, we developed a void-forming hydrogel using a feasible and effective approach for direct preparation of cell-laden porous hydrogels *via* a DLP-based bioprinting platform. The prepared bone tissue constructs with enhanced cell viability can be realized by rapidly projecting digital images with blue light. After establishment of the cellular hydrogels, the dextran polymer will be dissolved into the incubation media, leading to pore formation within the hydrogel constructs. The formed porous structure endowed the hydrogels with a favorable microenvironment for promoting the proliferation, migration, and spreading of the printed BMSCs.

To promote bone tissue regeneration, a cell-inspired microenvironment is needed for the regulation of encapsulated stem cells. Previous studies reported that YAP, a mechanosensitive transcriptional activator, shows a crucial role in regulating angiogenesis [39], immunomodulation [40], and tissue regeneration [41]. A study revealed that fast relaxing hydrogel with decreased mechanical properties was found to promote hMSCs spreading and YAP nuclear localization [16]. Recently, Lian et al. demonstrated that YAP staining appeared mainly in the nuclear portion when the BMSCs were seeded on the porous hydroxyapatite nanoparticles functionalized PLCL scaffolds [27]. In contrast, they observed significantly weakened YAP expression in BMSCs cultured on dense scaffolds. However, Ehlinger et al. highlighted the insensitivity of YAP translocation when dental pulp stem cells (DPSCs) were cultured on different substrate rigidity (from 1.5 KPa to 2.5 MPa) [42]. While the pore formation decreased strain and stress of the hydrogels in this study. Therefore, we hypothesized that whether our fabricated porous structure within the hydrogel had an effect on YAP signal pathway. In vitro testing revealed that YAP expression was significantly higher in encapsulated BMSCs within void-forming hydrogels than that in the standard hydrogels. Meanwhile, the void-forming hydrogels displayed capacities in facilitating YAP nuclear translocation. Although some research investigated that the porous hydrogels could facilitate cell spreading and proliferation of the directly encapsulated BMSCs, few disclosed the underlying molecular mechanisms [43]. Our studies provided an alternative approach to design 3D-bioprinted hydrogels for bone tissue engineering. On top of that, the up-regulation of YAP nuclear translocation enhanced ALP activity and gene expression of osteogenic markers when BMSCs cultured in osteogenic differentiation media, showing great potential in bone regeneration. However, the matrix elasticity has a significant regulation for bone regeneration. Nathaniel et al. reported that porous alginate hydrogel with an intermediate elastic modulus presented optimal bone regeneration [43]. Therefore, the elastic modulus of our void-forming hydrogel should be further optimized to match the mechanical environment.

The efficacy of the prepared hydrogels was evaluated in repairing the full-thickness craniotomy defects (6 mm in diameter). Our results displayed that, under the present experimental conditions, the skull was successfully reconstructed after treatment with BMSCs loaded void-forming hydrogels. After 2 months, histological analysis and immunofluorescence staining were performed to compare bone regeneration through the void-forming hydrogels with that supported by the standard hydrogels. After injury to the craniofacial bone, micro-CT contributes significant information in the evaluation of bone regeneration. The results indicated that the BMSCs loaded void-forming hydrogels realized a higher bone cover areas in cranial defect model of rats. Similarly, a large amount of newborn bone lacunas was observed to completely occupy the defects area and integrate tightly with the host bone tissues in the histoligical evulations. Meanwhile, higher osteo-related protein expression (OCN and COL-1) was confirmed in the void-forming group at 2 months. To conclude, this study presented a feasible and effective platform for 3D bioprinting of void-forming hydrogels in promoting skull reconstruction, paving the way for the next generation of BMSCs functionalized hydrogels.

5. Conclusion

A void-forming hydrogel was prepared by 3D bioprinting of the BMSCs mixed with an aqueous emulsion. The 3D-bioprinted porous hydrogel could significantly enhance the cell spreading, migration, and proliferation of the encapsulated BMSCs. More importantly, the niche created by the porous structure forced the YAP nuclear localization and facilitated the up-regulation of YAP targeted genes. In vivo testing revealed that the generated pores significantly promoted the 3D-bioprinted hydrogels in skull repair. The proposed strategy might represent a potential clinical alternative for skull regeneration, which also be expected to inspire the 3D bioprinting of functional biomaterials for tissue repair.

Credit author statement

J.T., J.S., and R.L. designed the experiments. J.T., S.Z., Y.Y., N.Z., and Y.T. performed the experiments. J.T., Y.W., Z.L., X.L., H.W., and S.Y. helped to analyze the results. J.T. wrote the manuscript. R.L. and J.S. supervised the project.

Declaration of competing interest

The authors declare that they have no known competing financial interests or personal relationships that could have appeared to influence the work reported in this paper.

Data availability

Data will be made available on request.

Acknowledgements

This study was supported by grants from the Clinical Innovation Project of Army Medical University (2019XLC2014), Science and Technology Foundation of Chongqing (cstc2021jcyj-msxmX0475 and cstc2021jcyj-msxmX0466), Chongqing Graduate Tutor Team Project (dstd201903), and Sichuan Science and Technology Program (2022YFQ0004).

Appendix A. Supplementary data

Supplementary data to this article can be found online at https://doi.org/10.1016/j.mtbio.2022.100487.

References

[1] L. Dejob, B. Toury, S. Tadier, L. Grémillard, C. Gaillard, V. Salles, Electrospinning of in situ synthesized silica-based and calcium phosphate bioceramics for applications in bone tissue engineering: a review, Acta Biomater. 123 (2021) 123–153, https://doi.org/10.1016/j.actbio.2020.12.032.
[2] G.L. Koons, M. Diba, A.G. Mikos, Materials design for bone-tissue engineering, Nat. Rev. Mater. 5 (2020) 584–603, https://doi.org/10.1038/s41578-020-0204-2.
[3] C. Hu, D. Ashok, D.R. Nisbet, V. Gautam, Bioinspired surface modification of orthopedic implants for bone tissue engineering, Biomaterials 219 (2019), 119366, https://doi.org/10.1016/j.biomaterials.2019.119366.
[4] Z. Wang, Y. Wang, J. Yan, K. Zhang, F. Lin, L. Xiang, L. Deng, Z. Guan, W. Cui, H. Zhang, Pharmaceutical electrospinning and 3D printing scaffold design for bone regeneration, Adv. Drug Deliv. Rev. 174 (2021) 504–534, https://doi.org/10.1016/j.addr.2021.05.007.
[5] T. Ahmad, H. Byun, J. Lee, S.K. Madhurakat Perikamana, Y.M. Shin, E.M. Kim, H. Shin, Stem cell spheroids incorporating fibers coated with adenosine and polydopamine as a modular building blocks for bone tissue engineering, Biomaterials 230 (2020), 119652, https://doi.org/10.1016/j.biomaterials.2019.119652.
[6] X. Liu, M. Chen, J. Luo, H. Zhao, X. Zhou, Q. Gu, H. Yang, X. Zhu, W. Cui, Q. Shi, Immunopolarization-regulated 3D printed-electrospun fibrous scaffolds for bone regeneration, Biomaterials 276 (2021), 121037, https://doi.org/10.1016/j.biomaterials.2021.121037.
[7] F. Shang, Y. Yu, S. Liu, L. Ming, Y. Zhang, Z. Zhou, J. Zhao, Y. Jin, Advancing application of mesenchymal stem cell-based bone tissue regeneration, Bioact. Mater. 6 (2021) 666–683, https://doi.org/10.1016/j.bioactmat.2020.08.014.
[8] W.L. Grayson, B.A. Bunnell, E. Martin, T. Frazier, B.P. Hung, J.M. Gimble, Stromal cells and stem cells in clinical bone regeneration, Nat. Rev. Endocrinol. 11 (2015) 140–150, https://doi.org/10.1038/nrendo.2014.234.
[9] Z.W. Wagoner, W. Zhao, Therapeutic implications of transplanted-cell death, Nature Biomedical Engineering 5 (2021) 379–384, https://doi.org/10.1038/s41551-021-00729-6.
[10] C. Loebel, J.A. Burdick, Engineering stem and stromal cell therapies for musculoskeletal tissue repair, Cell Stem Cell 22 (2018) 325–339, https://doi.org/10.1016/j.stem.2018.01.014.
[11] A.Y. Clark, K.E. Martin, J.R. García, C.T. Johnson, H.S. Theriault, W.M. Han, D.W. Zhou, E.A. Botchwey, A.J. García, Integrin-specific hydrogels modulate transplanted human bone marrow-derived mesenchymal stem cell survival, engraftment, and reparative activities, Nat. Commun. 11 (2020) 1–14, https://doi.org/10.1038/s41467-019-14000-9.
[12] Y. Liu, T. Li, M. Sun, Z. Cheng, W. Jia, K. Jiao, S. Wang, K. Jiang, Y. Yang, Z. Dai, L. Liu, G. Liu, Y. Luo, ZIF-8 modified multifunctional injectable photopolymerizable GelMA hydrogel for the treatment of periodontitis, Acta Biomater. (2022), https://doi.org/10.1016/j.actbio.2022.03.046.
[13] X. Zhao, S. Liu, L. Yildirimer, H. Zhao, R. Ding, H. Wang, W. Cui, D. Weitz, Injectable stem cell-laden photocrosslinkable microspheres fabricated using microfluidics for rapid generation of osteogenic tissue constructs, Adv. Funct. Mater. 26 (2016) 2809–2819, https://doi.org/10.1002/adfm.201504943.
[14] C. Liu, Q. Yu, Z. Yuan, Q. Guo, X. Liao, F. Han, T. Feng, G. Liu, R. Zhao, Z. Zhu, H. Mao, C. Zhu, B. Li, Engineering the viscoelasticity of gelatin methacryloyl (GelMA) hydrogels via small "dynamic bridges" to regulate BMSC behaviors for osteochondral regeneration, Bioact. Mater. (2022), https://doi.org/10.1016/j.bioactmat.2022.07.031.
[15] G.-L. Ying, N. Jiang, S. Maharjan, Y.-X. Yin, R.-R. Chai, X. Cao, J.-Z. Yang, A.K. Miri, S. Hassan, Y.S. Zhang, Aqueous two-phase emulsion bioink-enabled 3D bioprinting of porous hydrogels, Adv. Mater. 30 (2018), 1805460, https://doi.org/10.1002/adma.201805460.
[16] S. Tang, H. Ma, H.C. Tu, H.R. Wang, P.C. Lin, K.S. Anseth, Adaptable fast relaxing boronate-based hydrogels for probing cell–matrix interactions, Adv. Sci. 5 (2018) 1–8, https://doi.org/10.1002/advs.201800638.
[17] O. Chaudhuri, L. Gu, D. Klumpers, M. Darnell, S.A. Bencherif, J.C. Weaver, N. Huebsch, H. Lee, E. Lippens, G.N. Duda, D.J. Mooney, Hydrogels with tunable stress relaxation regulate stem cell fate and activity, Nat. Mater. 15 (2016) 326–334, https://doi.org/10.1038/nmat4489.
[18] G. Turnbull, J. Clarke, F. Picard, P. Riches, L. Jia, F. Han, B. Li, W. Shu, 3D bioactive composite scaffolds for bone tissue engineering, Bioact. Mater. 3 (2018) 278–314, https://doi.org/10.1016/j.bioactmat.2017.10.001.
[19] B. Charbonnier, M. Hadida, D. Marchat, Additive manufacturing pertaining to bone: hopes, reality and future challenges for clinical applications, Acta Biomater. 121 (2021) 1–28, https://doi.org/10.1016/j.actbio.2020.11.039.
[20] P. Jain, H. Kathuria, N. Dubey, Advances in 3D bioprinting of tissues/organs for regenerative medicine and in-vitro models, Biomaterials 287 (2022), 121639, https://doi.org/10.1016/j.biomaterials.2022.121639.
[21] Y. Jo, D.G. Hwang, M. Kim, U. Yong, J. Jang, Bioprinting-assisted tissue assembly to generate organ substitutes at scale, Trends Biotechnol. (2022) 1–13, https://doi.org/10.1016/j.tibtech.2022.07.001.
[22] M. Zhang, R. Lin, X. Wang, J. Xue, C. Deng, C. Feng, H. Zhuang, J. Ma, C. Qin, L. Wan, J. Chang, C. Wu, 3D printing of Haversian bone–mimicking scaffolds for multicellular delivery in bone regeneration, Sci. Adv. 6 (2020), https://doi.org/10.1126/sciadv.aaz6725 eaaz6725.
[23] J. Tao, J. Zhang, T. Du, X. Xu, X. Deng, S. Chen, J. Liu, Y. Chen, X. Liu, M. Xiong, Y. Luo, H. Cheng, J. Mao, L. Cardon, M. Gou, Y. Wei, Rapid 3D printing of functional nanoparticle-enhanced conduits for effective nerve repair, Acta Biomater. 90 (2019) 49–59, https://doi.org/10.1016/j.actbio.2019.03.047.
[24] J. Tao, S. Zhu, N. Zhou, Y. Wang, H. Wan, L. Zhang, Y. Tang, Y. Pan, Y. Yang, J. Zhang, R. Liu, Nanoparticle-stabilized emulsion bioink for digital light processing based 3D bioprinting of porous tissue constructs, Adv. Healthcare Mater. 11 (2022), 2102810, https://doi.org/10.1002/adhm.202102810.
[25] G. Brusatin, T. Panciera, A. Gandin, A. Citron, S. Piccolo, Biomaterials and engineered microenvironments to control YAP/TAZ-dependent cell behaviour, Nat. Mater. 17 (2018) 1063–1075, https://doi.org/10.1038/s41563-018-0180-8.
[26] P. Bandaru, G. Cefaloni, F. Vajhadin, K.J. Lee, H.J. Kim, H.J. Cho, M.C. Hartel, S. Zhang, W. Sun, M.J. Goudie, S. Ahadian, M.R. Dokmeci, J. Lee, A. Khademhosseini, Mechanical cues regulating proangiogenic potential of human mesenchymal stem cells through YAP-mediated mechanosensing, Small 16 (2020) 1–13, https://doi.org/10.1002/smll.202001837.
[27] M. Lian, B. Sun, Y. Han, B. Yu, W. Xin, R. Xu, B. Ni, W. Jiang, Y. Hao, X. Zhang, Y. Shen, Z. Qiao, K. Dai, A low-temperature-printed hierarchical porous sponge-like scaffold that promotes cell-material interaction and modulates paracrine activity of MSCs for vascularized bone regeneration, Biomaterials 274 (2021), 120841, https://doi.org/10.1016/j.biomaterials.2021.120841.
[28] C. Wang, W. Huang, Y. Zhou, L. He, Z. He, Z. Chen, X. He, S. Tian, J. Liao, B. Lu, Y. Wei, M. Wang, 3D printing of bone tissue engineering scaffolds, Bioact. Mater. 5 (2020) 82–91, https://doi.org/10.1016/j.bioactmat.2020.01.004.
[29] J. Nulty, F.E. Freeman, D.C. Browe, R. Burdis, D.P. Ahern, P. Pitacco, Y. Bin Lee, E. Alsberg, D.J. Kelly, 3D bioprinting of prevascularised implants for the repair of critically-sized bone defects, Acta Biomater. 126 (2021) 154–169, https://doi.org/10.1016/j.actbio.2021.03.003.
[30] Y. Xia, J. Sun, L. Zhao, F. Zhang, X.J. Liang, Y. Guo, M.D. Weir, M.A. Reynolds, N. Gu, H.H.K. Xu, Magnetic field and nano-scaffolds with stem cells to enhance bone regeneration, Biomaterials 183 (2018) 151–170, https://doi.org/10.1016/j.biomaterials.2018.08.040.
[31] H. Lin, J. Sohn, H. Shen, M.T. Langhans, R.S. Tuan, Bone marrow mesenchymal stem cells: aging and tissue engineering applications to enhance bone healing, Biomaterials 203 (2019) 96–110, https://doi.org/10.1016/j.biomaterials.2018.06.026.
[32] N. Golafshan, E. Vorndran, S. Zaharievski, H. Brommer, F.B. Kadumudi, A. Dolatshahi-Pirouz, U. Gbureck, R. van Weeren, M. Castilho, J. Malda, Tough magnesium phosphate-based 3D-printed implants induce bone regeneration in an equine defect model, Biomaterials 261 (2020), 120302, https://doi.org/10.1016/j.biomaterials.2020.120302.
[33] N. Ashammakhi, A. Hasan, O. Kaarela, B. Byambaa, A. Sheikhi, A.K. Gaharwar, A. Khademhosseini, Advancing frontiers in bone bioprinting, Adv. Healthcare Mater. 8 (2019) 1–24, https://doi.org/10.1002/adhm.201801048.
[34] A. Lee, A.R. Hudson, D.J. Shiwarski, J.W. Tashman, T.J. Hinton, S. Yerneni, J.M. Bliley, P.G. Campbell, A.W. Feinberg, 3D bioprinting of collagen to rebuild components of the human heart, Science 365 (2019) 482–487, https://doi.org/10.1126/science.aav9051.
[35] N. Kleger, M. Cihova, K. Masania, A.R. Studart, J.F. Löffler, 3D printing of salt as a template for magnesium with structured porosity, Adv. Mater. 31 (2019), 1903783, https://doi.org/10.1002/adma.201903783.
[36] B. Wu, C. Yang, Q. Xin, L. Kong, M. Eggersdorfer, J. Ruan, P. Zhao, J. Shan, K. Liu, D. Chen, D.A. Weitz, X. Gao, Attractive pickering emulsion gels, Adv. Mater. (2021), 2102362, https://doi.org/10.1002/adma.202102362, 1–8.
[37] S.T. Koshy, T.C. Ferrante, S.A. Lewin, D.J. Mooney, Injectable, porous, and cell-responsive gelatin cryogels, Biomaterials 35 (2014) 2477–2487, https://doi.org/10.1016/j.biomaterials.2013.11.044.
[38] Z. Luo, G. Tang, H. Ravanbakhsh, W. Li, M. Wang, X. Kuang, C.E. Garciamendez-Mijares, L. Lian, S. Yi, J. Liao, M. Xie, J. Guo, Z. Zhou, Y.S. Zhang, Vertical extrusion

cryo(bio)printing for anisotropic tissue manufacturing, Adv. Mater. 34 (2022), 2108931, https://doi.org/10.1002/adma.202108931.

[39] X. Wang, A. Freire Valls, G. Schermann, Y. Shen, I.M. Moya, L. Castro, S. Urban, G.M. Solecki, F. Winkler, L. Riedemann, R.K. Jain, M. Mazzone, T. Schmidt, T. Fischer, G. Halder, C. Ruiz de Almodóvar, YAP/TAZ orchestrate VEGF signaling during developmental angiogenesis, Dev. Cell 42 (2017) 462–478, https://doi.org/10.1016/j.devcel.2017.08.002, e7.

[40] V.S. Meli, H. Atcha, P.K. Veerasubramanian, R.R. Nagalla, T.U. Luu, E.Y. Chen, C.F. Guerrero-Juarez, K. Yamaga, W. Pandori, J.Y. Hsieh, T.L. Downing, D.A. Fruman, M.B. Lodoen, M.V. Plikus, W. Wang, W.F. Liu, YAP-mediated mechanotransduction tunes the macrophage inflammatory response, Sci. Adv. 6 (2020) 1–14, https://doi.org/10.1126/sciadv.abb8471.

[41] H. Jeanette, L.N. Marziali, U. Bhatia, A. Hellman, J. Herron, A.M. Kopec, M.L. Feltri, Y. Poitelon, S. Belin, YAP and TAZ regulate Schwann cell proliferation and differentiation during peripheral nerve regeneration, Glia 69 (2021) 1061–1074, https://doi.org/10.1002/glia.23949.

[42] C. Ehlinger, E. Mathieu, M. Rabineau, V. Ball, P. Lavalle, Y. Haikel, D. Vautier, L. Kocgozlu, Insensitivity of dental pulp stem cells migration to substrate stiffness, Biomaterials 275 (2021), 120969, https://doi.org/10.1016/j.biomaterials.2021.120969.

[43] N. Huebsch, E. Lippens, K. Lee, M. Mehta, S.T. Koshy, M.C. Darnell, R.M. Desai, C.M. Madl, M. Xu, X. Zhao, O. Chaudhuri, C. Verbeke, W.S. Kim, K. Alim, A. Mammoto, D.E. Ingber, G.N. Duda, D.J. Mooney, Matrix elasticity of void-forming hydrogels controls transplanted-stem-cell-mediated bone formation, Nat. Mater. 14 (2015) 1269–1277, https://doi.org/10.1038/nmat4407.